CHAPTER 2

Materials and Methods

2.1. Introduction

This chapter deliberates the complete description of materials and experimental methodologies for the synthesis of fluorescent carbon quantum dots (CQDs) which have been used for sensing applications. The current chapter also discusses about the various modern characterization techniques such as Fourier Transform Infrared (FTIR) Spectroscopy, UV-visible spectroscopy, Fluorescence Spectroscopy, X-Ray Diffraction (XRD), Transmission Electron Microscopy (TEM), Energy-Dispersive X-Ray Spectroscopy (EDAX), Selected Area Electron Diffraction Pattern (SAED), and X-Ray Photoelectron Spectroscopy (XPS). In addition to this, the detail procedures of various applications of CQDs performed in the detection assay of cobalt (II), mercury (II), and glutathione (GSH) is also discussed briefly. The present chapter also includes the *in vitro* live cell imaging assay on human lung cancer cells (A549). In addition to this, it further covers the application of CQDs as peroxidase like activity and detail about the determination of fluorescence quantum yield, Stern-Volmer plot and detection limit are also deliberated. The present chapter also stated about the preparation of stock solution of different analytes for their application.

2.2. Materials

The present study is established the development of economically viable and energy efficient route for the CQDs synthesis. In this research work, the CQDs were synthesized by both the precursors chemical as well as biological for the detection of mercury (II), cobalt (II), and GSH. The required chemicals in the application part of this study were of AR grade and used without any further alteration and listed in the **Table 2.1**. Throughout the whole experiments, ultrapure water was utilized as a green solvent.

Table 2.1 List of Chemicals

S. No.	Name	Chemical formula	Physical state	Manufacturer
1	Ferric Chloride	$FeCl_3$	Solid	SD Fine-Chem Ltd.
2	Manganese Chloride	$MnCl_2$	Solid	SD Fine-Chem Ltd.
3	Lead Chloride	$PbCl_2$	Solid	SD Fine-Chem Ltd.
4	Iron (II) Chloride Tetrahydrate	$FeCl_2.4H_2O$	Solid	SD Fine-Chem Ltd.
5	Cobaltous Nitrate	$Co(NO_3)_2.6H_2O$	Solid	SD Fine-Chem Ltd.
6	Arsenic tri-oxide	As_2O_3	Solid	SD Fine-Chem Ltd.
7	Calcium Chloride	$CaCl_2$	Solid	SD Fine-Chem Ltd.
8	Nickel Chloride	$NiCl_2.6H_2O$	Solid	SD Fine-Chem Ltd.
9	Zinc Nitrate	$Zn(NO_3)_2$	Solid	SD Fine-Chem Ltd.
10	Cadmium Nitrate	$Cd(NO_3)_2.4H2O$	Solid	SD Fine-Chem Ltd.
11	Aluminium Nitrate	$Al(NO_3)_3.9H_2O$	Solid	SD Fine-Chem Ltd.
12.	Sodium chloride	NaCl	Solid	SD Fine-Chem Ltd.
13	Potassium permanganate	$KMnO_4$	Solid	Sigma Aldrich
14	Mercuric Nitrate	$Hg(NO_3)_2.H_2O$	Solid	SD Fine-Chem Ltd.
15	Cupric nitrate	$Cu(NO_3)_2.3H_2O$	Solid	SD Fine-Chem Ltd.
16	Ethanol	C_5H_5OH	Liquid	Sigma Aldrich
17	Magnesium Chloride	$MgCl_2$	Solid	SD Fine-Chem Ltd.
18	Isopropyl alcohol (IPA)	C_3H_7OH	Liquid	SD fine-chem Ltd.
19	Thiourea	C_3H_6S	Solid	SD fine-chem Ltd.
20	Glucose	$C_6H_{12}O_6$	Solid	Sigma Aldrich
21	Sulfuric acid	H_2SO_4	Liquid	Sigma Aldrich
22	Methanol	CH_3OH	Liquid	SD fine-chem Ltd.
23	Phosphoric acid	H_3PO_4	Liquid	Sigma Aldrich
24	Ascorbic Acid	$C_6H_8O_6$	Solid	Sigma Aldrich
25	Sodium hydroxide	NaOH	Solid	SD Fine-Chem Ltd.
26	Nitric Acid	HNO_3	Liquid	SD Fine-Chem Ltd.
27	Hydrogen peroxide	H_2O_2,	Liquid	Sigma Aldrich
28	Hydrochloric acid	HCl	Liquid	SD Fine-Chem Ltd.
29	Ammonium persulphate (APS)	$(NH_4)_2S_2O_8$	Solid	SD Fine-Chem Ltd.
30	Di-sodium hydrogen phosphate	Na_2HPO_4	Solid	Merck
31	Potassium Chloride	KCl	Liquid	Merck
32	Acetone	$(CH_3)_2CO$	Liquid	SD Fine-Chem Ltd.
33	Quinine sulphate	C40H50N4O8S	solid	Sigma Aldrich
34	Tetramethylbenzidine (TMB)	$C_{16}H_{20}N_2$	Solid	Sigma Aldrich
35	Terephthalic acid	C_6H_4-1,4-$(CO_2H)_2$	solid	Sigma Aldrich
36	Glycine (Gly)	$C_2H_5NO_2$	Solid	Sigma Aldrich
37	Valine (Val)	$C_5H_{11}NO_2$	Solid	Sigma Aldrich
38	Alanine (Ala)	$C_3H_7NO_2$	Solid	Sigma Aldrich

39	Proline (Pro)	$C_5H_9NO_2$	Solid	Sigma Aldrich
40	Leucine (Leu)	$C_6H_{13}NO_2$	Solid	Sigma Aldrich
41	Lysine (Lys)	$C_6H_{14}N_2O_2$	Solid	Sigma Aldrich
42	Isoleucine (Ile)	$C_6H_{13}NO_2$	Solid	Sigma Aldrich
43	Serine (Ser)	$C_3H_7NO_3$	Solid	Sigma Aldrich
44	Threonine (Thr)	$C_4H_9NO_3$	Solid	Sigma Aldrich
45	Glutathione (GSH)	$C_{10}H_{17}N_3O_6S$	Solid	Sigma Aldrich
46	Phenylalanine (Phe)	$C_9H_{11}NO_2$	Solid	Sigma Aldrich
47	Tryptophan (Trp)	$C_{11}H_{12}N_2O_2$	Solid	Sigma Aldrich
48	Tyrosin (Tyr)	$C_9H_{11}NO_3$	Solid	Sigma Aldrich
49	Methionine (Met)	$C_5H_{11}NO_2S$	Solid	Sigma Aldrich
50	Cysteine (Cys)	$C_3H_7NO_2S$	Solid	Sigma Aldrich
51	Glutamic acid (Glu)	$C_5H_9NO_4$	Solid	Sigma Aldrich
52	Arginine (arg)	$C_6H_{14}N_4O_2$	Solid	Sigma Aldrich
53	Glutamine (Gln)	$C_5H_{10}N_2O_3$	Solid	Sigma Aldrich
54	Aspartic acid (asp)	$C_4H_7NO_4$	Solid	Sigma Aldrich
55	Asparagine (asn)	$C_4H_8N_2O_3$	Solid	Sigma Aldrich
56	Methyl alcohol (MA)	CH_3OH	Liquid	SD fine-chem Ltd.
57	Dimethyl sulfoxide (DMSO)	$(CH_3)_2SO$	Liquid	SD fine-chem Ltd.
58	Dulbecco's Modified Eagle's medium	*******	liquid	Invitrogen Corporation
59	Fetal bovine serum	*******	liquid	Gibco
60	Penicillin	*******	liquid	Gibco
61	Streptomycin	*******	liquid	Gibco
62	A549 cell	*******	liquid	National Centre for Cell Science (NCCS), Pune, India

2.3. Methods

2.3.1. Synthesis of carbon quantum dots (CQDs)

Based on the various organic precursors, we have synthesized CQDs from the pure chemical as well as natural organic precursors via one step hydrothermal treatment. Typically, in the synthesis process of CQDs, precursors were properly dispersed in the ultrapure water and sealed in a Teflon-lined stainless steel autoclaved and kept in oven at high temperature up to 3–5 hours. Subsequently, reaction vessel was cooled to room temperature (RT) and the obtained dark brown solution was filtered and centrifuge at 10,000 rpm for 15 minutes to remove the larger and agglomerated particles. Then, the obtained supernatant was filtered against the dialysis membrane and syringe filter to obtain the pure CQDs. The detail procedures for CQDs synthesis are stated in chapter 3, 4, 5, and 6 under the experimental section.

2.3.2. Synthesis of MnO_2 nanosheets

Typically, 2 mL of $KMnO_4$ solution (10 mM) was diluted with the 12 mL of ultrapure distilled water and subsequently 6 mL of glucose solution (100 mM) was added into it. The deep purple color solution of $KMnO_4$ was instantly kept for the ultra-sonication process at 35 ^oC up to 15 min. The dark brown colloidal solution was cooled down at room temperature. The obtained solution was centrifuged at 15,000 rpm up to 25 min and the supernatant part was discarded and resuspended in water. This process was repeated 3–4 times to sanitize the MnO_2 nanosheets. The concentration of MnO_2 nanosheets was adjusted to 200 μg/mL and the obtained sample was kept in 4 mL of distilled water in an incubator at 4 ^oC until further apply.

2.4. Preparation of standard

2.4.1. Preparation of standard solution of glutathione (GSH)

The stock solution of GSH (1x 10^{-2} M) were prepared by dissolving 30.7 mg of GSH in 10 mL of ultrapure water in volumetric flask. The lower concentration of GSH were prepared by the serial dilution method.

2.4.2. Preparation of standard solution of other reducing agents

The stock solution of other reducing agent such as various amino acid and glucose were prepared in similar manner by dissolving appropriate quantity of each amino acid in ultrapure water separately.

2.4.3. Preparation of standard solution of Hg^{2+}

The stock solution of Hg^{2+} with concentration of 1x 10^{-2} M were prepared by dissolving 34.2 mg of $Hg(NO_3)_2$. H_2O was dissolved in 10 mL of ultrapure water in volumetric flask. The desired concentration of Hg^{2+} solution were obtained from the stock solution by serial dilution method.

2.4.4. Preparation of standard solution of 3,3′,5,5′-Tetramethylbenzidine (TMB)

The stock solution of TMB with concentration of 1x 10^{-2} M was prepared by dissolving 24.0 mg of TMB in 10 mL of ethanol in a volumetric flask. The desired concentration of TMB was obtained through serial dilution of stock solution in ethanol.

2.5. *In vitro* cell imaging method

2.5.1. Cell viability assay

The cell viability assay of N,S–CQD–MnO_2 was performed by using 3-(4,5-dimethyl thiazol-2yl)- 2,5-diphenyl tetrazolium bromide (MTT) as a standard protocol by using A549 human lung cancer cell line (Chapter 4). The A549 cells were preserved in the Dulbecco's Modified Eagle Medium, supplemented (Gibco) with the 10% fetal bovine serum at 37 °C in 5% CO_2 in a humidified atmosphere. The A549 cells were grown in 96-well plate (1.0×10^4 cells per well) and allowed to stick overnight at 37 °C. Then, the medium was removed and the cells were incubated with the 50 μL of different N,S–CQD–MnO_2 concentration (20, 40, 60, 80, 100, and 200 μg/mL) for 24 hours. The medium was then removed and 250 μL of DMSO was added to dissolve the formazan crystals. Subsequently, the absorbance spectra were traced at 570 nm in a micro-plate reader. The cytotoxicity and viability were calculated by the following given **equation 2.1** and **2.2**.

$$\text{Cell viability (\%)} = \text{Mean OD/control OD} \times 100 \qquad 2.1$$

$$\text{Cytotoxicity (\%)} = 100 - \text{cell viability (\%)} \qquad 2.2$$

2.5.2. *In vitro* cellular imaging

Lung cancer cells (A549) were seeded in tissue culture plates ($1x10^4$ cells per well) and incubated for 24 hours at 37 ^oC in CO_2 atmosphere. Then, the exhausted media was rejected and cells were washed with the PBS buffer (10 mM at pH 7.4). Subsequently, the cells were treated with the 400 μL fresh Dulbecco's Modified Eagle Medium, supplemented (Gibco) containing 70 μg/mL nanoprobe solution. After incubating overnight for 12 hours, the A549 cells were further washed with the PBS and monitored for the *in vitro* fluorescence

cellular imaging by using inverted fluorescence microscope. The detailed is given in chapter 4.

2.6. Calculations

2.6.1. Quantum yield (QY) determination

The quantum yield of fluorescent carbon quantum dots was also investigated with respect to the quinine sulphate as a s standard solution (QY = 54% at 360 nm excitation). The absorbance (below 0.1) of quinine sulphate solution in 0.1M H_2SO_4 was measured and fluorescence spectrum of the same solution was carried out and their fluorescence integrated intensity was calculated. The same measurement was performed for fluorescent material and their quantum yield were determined from the (**equation 2.3**).

$$QY = QY_s \cdot \frac{I}{I_s} \cdot \frac{A_s}{A} \cdot \frac{\eta^2}{\eta_s^2} \qquad 2.3$$

Where 'QY' stand for the quantum yield, 'I' denotes for the integrated fluorescence emission intensity, 'A' for the optical density, 'η' refers to the refractive index of the solvent (for the ultrapure water as solvent $\eta/\eta_s = 1$), and 's' stands for the standard used.

2.6.2. Determination of limit of detection (LOD)

The limit of detection (LOD) is the least concentration of metal ions and biomolecules, measured based on a certain level of confidence. It can be calculated by using the following formula

$$LOD = 3\sigma/s \qquad 2.4$$

Where, "σ" is the standard deviation of the blank and "s" is the slope of the calibration sensitivity

2.6.3. Determination of Stern-Volmer constant

The Stern-Volmer quenching constant was calculated using following equation

$$(F_0/F)\text{-}1 = K_{sv}\,[Q] \qquad 2.5$$

where "F" is the fluorescence intensity of sensor in the presence of analyte and "F_0" is the fluorescence intensity of sensor. "K_{sv}" is the Stern-Volmer quenching constant and "[Q]" is the concentration of quencher.

2.7. Instrumentations

The as-prepared CQDs were characterized by the various instrumentation technique which are deliberated briefly.

2.7.1. Transmission Electron Microscopy (TEM)

TEM is a powerful electron microscope that uses a beam of electrons to focus on a specimen producing a highly magnified and detailed image of the specimen. The magnification power is over 2 million times better than that of the light microscope, producing the image of the specimen which enables easy characterization of the image in its morphological features, compositions and crystallization information is also detailed. In this technique, a heated tungsten filament in the electron gun produces electrons that get focus on the specimen by the condenser lenses **(Figure 2.1)**. On reaching the specimen, the specimen scatters the electrons focusing them on the magnetic lenses forming a large clear image, and if it passes through a fluorescent screen it forms a polychromatic image. The denser the specimen, the more the electrons are scattered forming a darker image because fewer electron reaches the screen for visualization while thinner, more transparent specimens appear brighter.

TEM operates on the same basic principles as the light microscope but uses electrons instead of light. Since the electrons have both wave and particle nature and the de Broglie wavelength of electrons are significantly smaller than that of light and so they have higher resolution capability. This enables the instrument's user to examine fine detail-even as small as a single column of atoms, which is tens of thousands times smaller than the smallest resolvable object in a light microscope. TEM forms a major analysis method in a range of scientific fields, in physical, chemical and biological sciences. At smaller magnifications

TEM image is contrast due to absorption of electrons in the material, as well as thickness and composition of the material. At higher magnifications complex wave interactions modulate the intensity of the image, requiring expert analysis of observed images. Alternate modes of use allow for the TEM to observe modulations in chemical identity, crystal orientation, electronic structure and sample induced electron phase shift as well as the regular absorption based imaging.

In the present study, the TEM analysis of the sample were performed on TECNAI 20 G2-Electron Microscope operated at accelerating voltage 200 kV (**Figure 2.2**). The samples were prepared by simply mounted the dilute solution of the sample on carbon coated TEM grid and dried under table lamp for 5 h after that vacuum dried overnight.

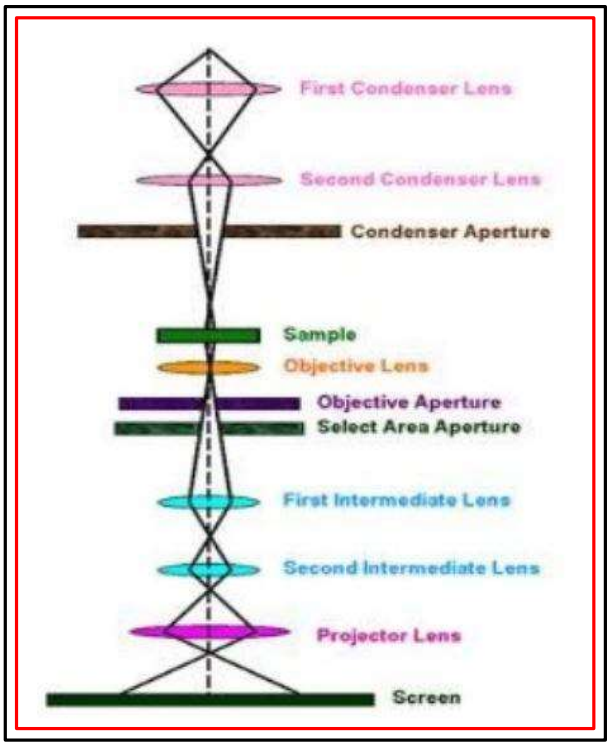

Figure 2.1 Schematic representation of principle of Transmission electron microscopy.

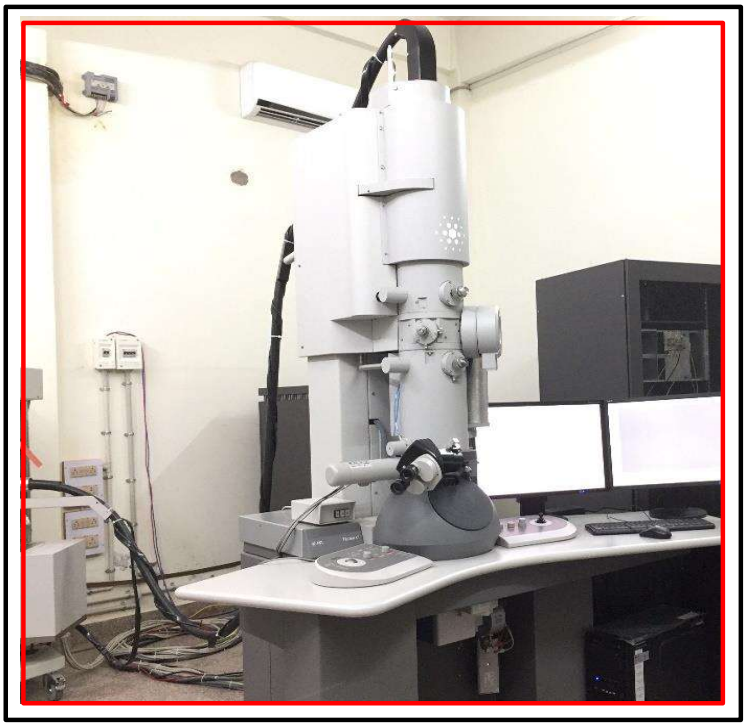

Figure 2.2 Photograph of Transmission electron microscopy (TEM).

2.7.2. X-ray Diffraction (XRD)

X-ray diffraction (XRD) is now a common technique for the study of crystal structures and atomic spacing. XRD is based on constructive interference of monochromatic X-rays and a crystalline sample. These X-rays are generated by a cathode ray tube, filtered to produce monochromatic radiation, collimated to concentrate, and directed toward the sample.

The interaction of the incident rays with the sample produces constructive interference (and a diffracted ray) when conditions satisfy Bragg's Law (**equation 2.6**).

$$n\lambda=2d \sin \theta \qquad 2.6$$

Where, n is an integer value, λ represents the wavelength of X-rays, d is interplanar spacing generating the diffraction, and θ is the diffraction angle.

This law relates the wavelength of electromagnetic radiation to the diffraction angle and the lattice spacing in a crystalline sample. These diffracted X-rays are then detected, processed and counted. By scanning the sample through a range of 2θ angles, all possible diffraction directions of the lattice should be attained due to the random orientation of the powdered material **(Figure 2.3)**.

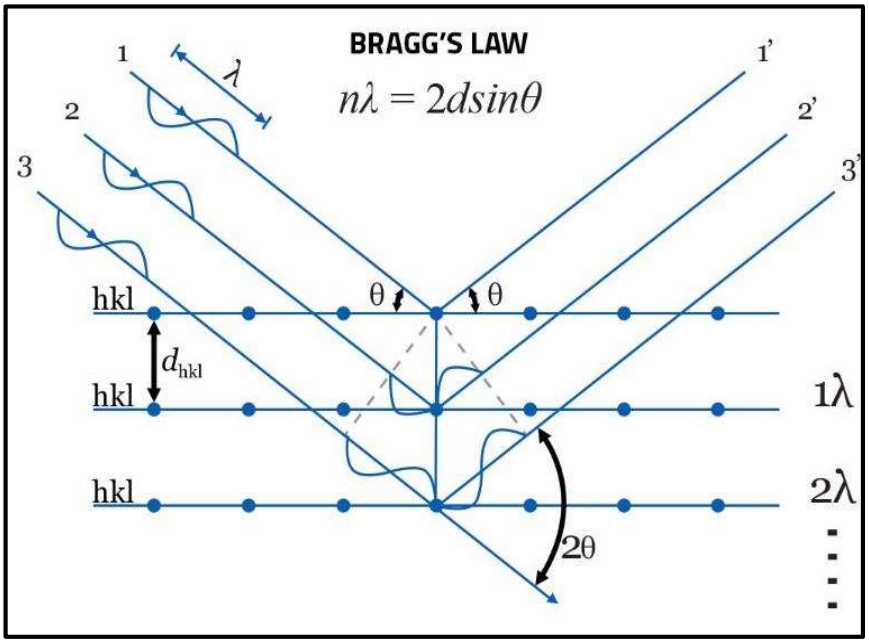

Figure 2.3 X-rays diffraction by crystal plane (Bragg's law)

In the typical X-ray diffraction an X-ray are generated by cathode ray tube and the filtered monochromatic radiation collimated and directed toward the sample. The interaction of the incident rays with the sample produces constructive interference i.e. diffracted ray when it satisfies the Bragg's law. These diffracted X−rays are then detected, processed and counted and all possible diffraction directions of the lattice should be attained due to the random orientation of the powdered material by scanning the sample through a range of 2θ angles.

X-ray diffractometers consist of three basic elements: an X-ray tube, a sample holder, and an X-ray detector. X-rays are generated in a cathode ray tube by heating a filament to produce electrons, accelerating the electrons toward a target by applying a voltage, and bombarding the target material with electrons. When electrons have sufficient energy to dislodge inner shell electrons of the target material, characteristic X-ray spectra are produced. These spectra consist of several components, the most common being K_α and K_β. K_α consists, in part, of $K_{\alpha1}$ and $K_{\alpha2}$. $K_{\alpha1}$ has a slightly shorter wavelength and twice the intensity as $K_{\alpha2}$. The specific wavelengths are characteristic of the target material (Cu, Fe, Mo, Cr). Filtering, by foils or crystal monochromator, is required to produce monochromatic X-rays needed for diffraction. $K_{\alpha1}$and $K_{\alpha2}$ are sufficiently close in wavelength such that a weighted average of the two is used. Copper is the most common target material for single-crystal diffraction, with CuK_α radiation = 1.5418Å. These X-rays are collimated and directed onto the sample. As the sample and detector are rotated, the intensity of the reflected X-rays is recorded. When the geometry of the incident X-rays impinging the sample satisfies the Bragg Equation, constructive interference occurs and a peak in intensity occurs. A detector records and processes this X-ray signal and converts the signal to a count rate which is then output to

a device such as a printer or computer monitor. The schematic representation and photograph of XRD are given in **Figure 2.4 and 2.5**.

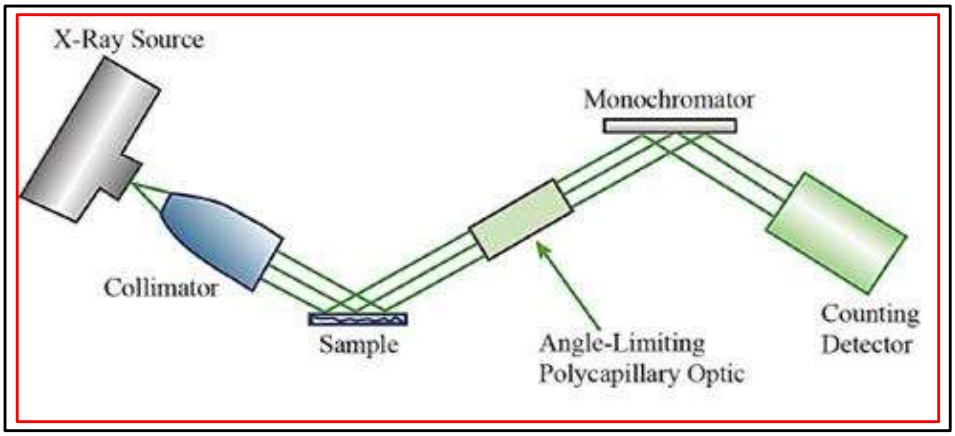

Figure 2.4 Schematic representation of principle of X-Ray diffraction spectroscopy (XRD).

Figure 2.5 Photograph of X-Ray diffraction spectroscopy (XRD).

2.7.3. Fourier Transform Infrared Spectroscopy (FTIR)

FTIR spectroscopy is a technique which is used to recognize the presence of different functional groups in molecules or compounds either organic or inorganic. It is a powerful tool for identifying types of chemical bonds in a molecule by producing an infrared absorption spectrum that is like a molecular "fingerprint". The term Fourier Transform Infrared Spectroscopy (FTIR) refers to a development in the manner in which the data is collected and converted from an interference pattern to a spectrum. The working principle are based on Michelson interferometer which consist of beam splitter, a fixed mirror and a movable mirror that translate back and forth precisely. The radiation from the source strike to the beam splitter and separate into two beam. One beam is transmitted through the beam splitter and goes to the static mirror whereas second beam is reflected off the beam splitter to the moving mirror. The fixed and moving mirrors reflect the radiation back to the beam splitter. Again, half of this reflected radiation is transmitted and half is reflected at the beam splitter, resulting in one beam passing through the sample and detected by the detector and spectra are display on computer and the second back to the source.

In our study, the FTIR spectra of the sample were conducted by using the instrument “PerkinElmer Spectrum 100”. The radiation sources passed through KBr window and transmitted data were collected by $LiTaO_3$ detector and spectra were displayed in transmitted mode. The pellets of the sample were prepared by mixing the sample with KBr in the ratio of 1:100 and the sample pellets were scanned in the range of 400-4000 cm^{-1} with the spectral resolution of 4.0 cm^{-1} and scan speed 0.2 cm/sec. The working principle and photograph of FTIR spectrophotometer are given in **Figure 2.6**.

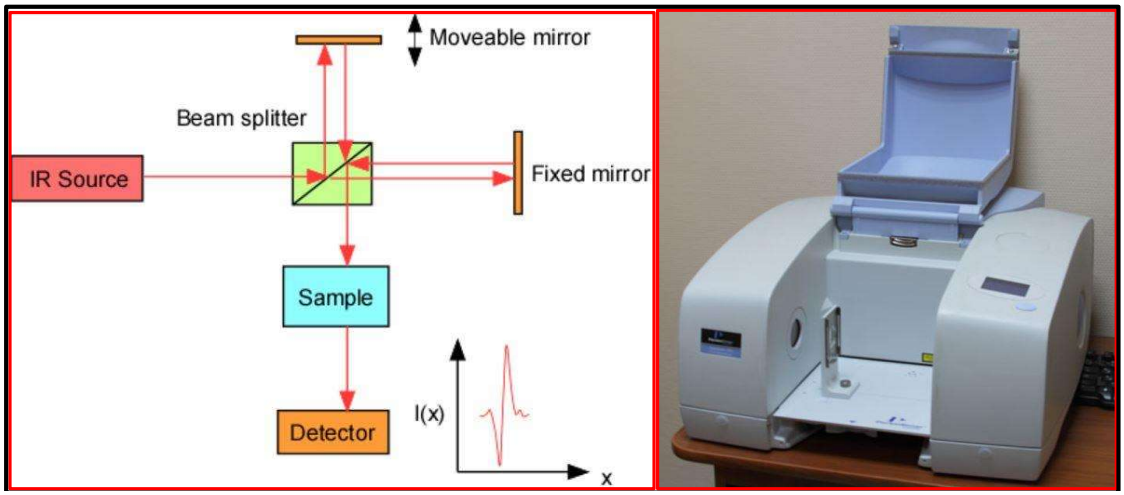

Figure 2.6 Schematic representation of working of Fourier transform infrared (FTIR) spectrophotometer and its photograph.

2.7.4. X-ray Photoelectron Spectroscopy (XPS)

X-ray Photoelectron Spectroscopy (XPS) is the most widely used surface analysis technique because it can be applied to a broad range of materials and provides valuable quantitative and chemical state information from the surface of the material being studied. XPS is a useful measurement technique because it is not only shows what elements are within a sample but also; what other elements they are bonded to. The average depth of analysis for an XPS measurement is approximately 5 nm. The working principle of XPS analysis is based on irradiation of target material with X-ray of sufficient energy in ultrahigh vacuum condition around 10^{-9} millibar (mbar); results in electrons in specific bound states to be excited. Some of the photo-ejected electrons inelastically scatter through the sample enroute to the surface, while others undergo prompt emission and suffer no energy loss in escaping the surface and into the surrounding vacuum. Once these photo-ejected electrons are in the vacuum, they are collected by an electron analyzer that measures their kinetic

energy. An electron energy analyzer produces an energy spectrum of intensity (number of photo-ejected electrons versus time) versus binding energy (the energy the electrons had before they left the atom). Each prominent energy peak on the spectrum corresponds to a specific element. The intensity of the peaks can also tell how much of each element is in the sample. Each peak area is proportional to the number of atoms present in each element and chemical composition is obtained by calculating the respective contribution of each peak area.

The main components of a XPS system include a source of X-rays, monochromator an ultra-high vacuum (UHV) stainless steel chamber with UHV pumps, an electron collection lens, an electron energy analyzer, an electron detector system, and a moderate vacuum sample introduction chamber. For the X-ray source commonly Al Kα or Mg Kα is used. The schematic representation of the XPS is given in **Figure 2.7**.

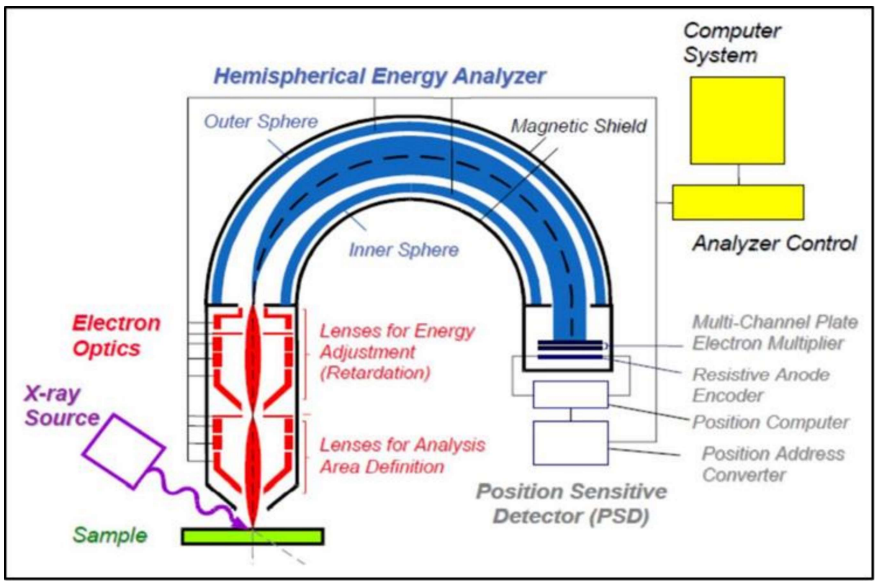

Figure 2.7 Working principle of X-ray photoelectron spectroscopy (XPS).

In the present study XPS analysis of the sample was measured on "AMICUS, kratos, Analytical, A Shimadzu spectrometer" with Mg Kα excitation (1253.6 eV) radiation **(Figure 2.8).**

Figure 2.8 Typical photograph of XPS instrument.

2.7.5. Zeta Potential

Zeta potential is the potential difference between the dispersion medium and the stationary layer of fluid attached to the dispersed particle. It is usually denoted using the Greek letter zeta (ζ), and represented in units volts (V) or millivolts (mV). The zeta potential is a key indicator of the stability of colloidal dispersions. The magnitude of the zeta potential indicates the degree of electrostatic repulsion between adjacent, similarly charged particles in a dispersion. The value of zeta potential typically ranges from +100 mV to -100 mV. The ζ – potential explains the reason behind the dispersion, aggregation or flocculation. So, colloids with high zeta potential (negative or positive) are electrically stabilized while colloids with low zeta potentials tend to coagulate or flocculate. Therefore, it can be used to improve the formulation of dispersions, emulsions and suspensions. It is highly influence by the pH of the

solution. It is positive at low pH and negative at high pH. The working principle and the digital image of the zetasizer are given in **Figure 2.9**.

In the current investigation, the Zeta potential were measured by using two different instruments Malvern Zetasizer (Malvern Instruments, Ltd.) and NanoPlus HD.

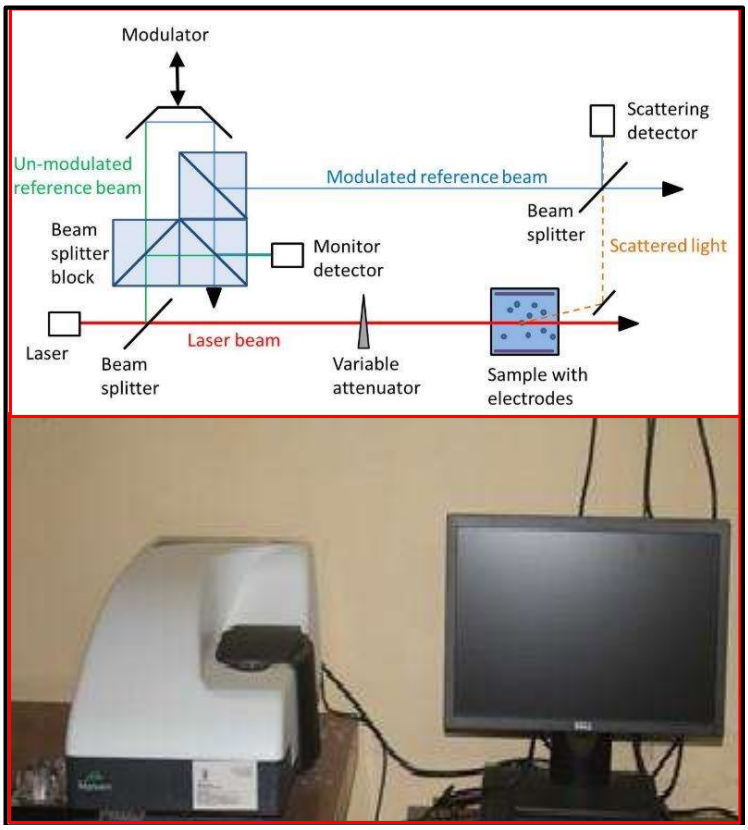

Figure 2.9. Working principle of Zetasizer and its photograph.

2.7.6. UV-visible Spectroscopy

UV-Visible spectroscopy is the study of interaction of light with the chemical compounds. When a beam of light passes through a chemical compound, it results in absorption, transmission and reflection of light over a certain range of wavelength. Spectrophotometry is used to measure the amount of light absorbed or transmitted by the chemical compounds. The transmittance is the ratio of the intensity of the light entering the

sample (I_0) to that exiting the sample (I_t) at a particular wavelength and expressed as percentage transmittance (%T) (**Equation 2.7**).

$$\%T = \left(\frac{I_0}{I_t}\right) \times 100 \qquad 2.7$$

The negative logarithm of the transmittance is the absorbance (A) (**Equation 2.8**).

$$A = -\log T \qquad 2.8$$

The UV-visible range of the electromagnetic radiation ranges from 190-700 nm. Lambert's and Beer's laws are most important principles in absorption analysis. Lambert's law states that the fraction of radiation absorbed is independent of the intensity of the radiation and Beer's law states that absorption is proportional to the concentration of absorbing molecules. Combining these two laws, we can derive the Beer-Lambert's Law (**Equation 2.9)**.

$$\log_{10}\left(\frac{I_0}{I_t}\right) = \varepsilon c l \qquad 2.9$$

Where 'I_0' is the intensity of the incident radiation and 'I_t' is the intensity of the transmitted radiation. 'ε' is the molar absorption coefficient which is constant for each absorbing material, and having the units mol^{-1} dm^3 cm^{-1}, 'l' is the path of the length in cm, 'c' is the concentration of the absorbing molecule in mol dm^{-3} non-bonding orbitals (lone pair electrons) from lower to higher energy levels. The non-bonding orbitals are higher in energy comparatively π bonding orbitals which in turn are higher in energy than σ bonding orbitals. When the electromagnetic radiation of the correct frequency is absorbed, a transition occurs from one of these orbitals to an empty orbital, i.e. σ* or π*. The differences of energy among the orbitals depend on the bonding system and atoms present. Most of the transitions from bonding orbitals are of too short a wavelength (too high a frequency) to measure easily.

Therefore, most of the absorptions observed involve only π→π*, n→σ* and n→π* transitions. A common exception to this is the d→d transition of d-block element complexes. In general, the UV-visible spectrometer consist two light sources, a monochromator, and a detector. Generally, the light sources are deuterium lamp and tungsten lamp which emit electromagnetic radiation in UV region and in the visible region of spectrum respectively. The important role played by the monochromator is the spreading of the beam of light into its component wavelengths. The detector is generally a photomultiplier tube (photodiodes in modern instruments). The possible electronic transitions and schematic diagram in UV-visible spectroscopy are given in **Figure 2.10 and 2.11**.

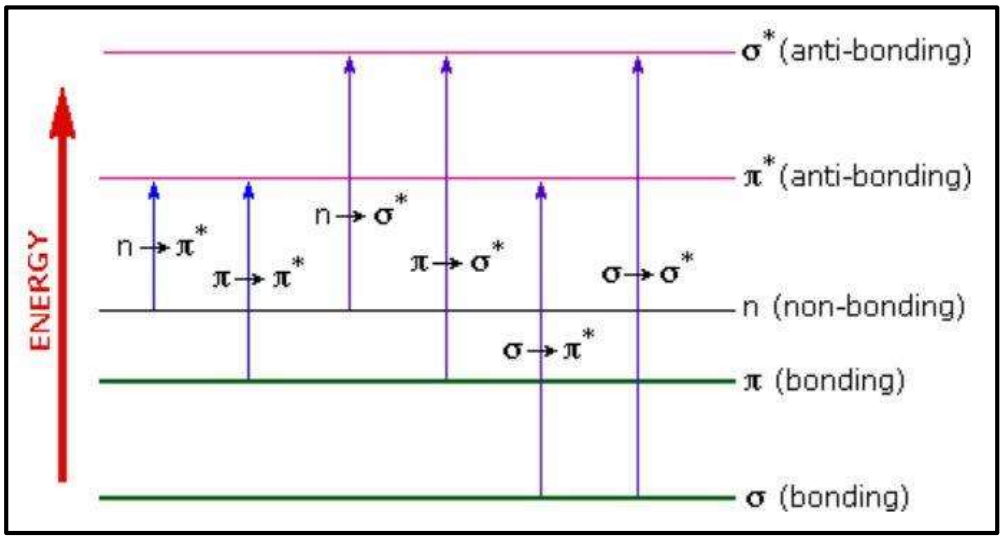

Figure 2.10 Schematic representation of possible electronic transitions in UV-visible spectroscopy.

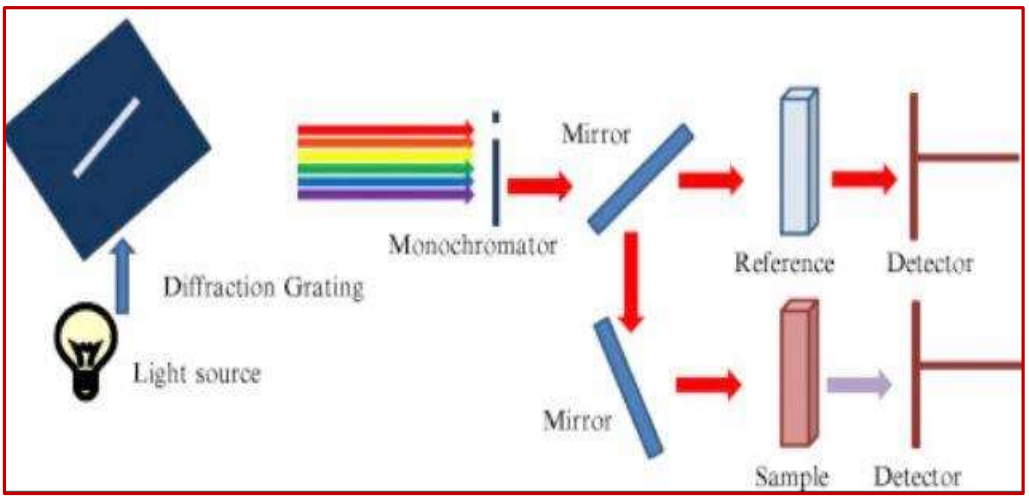

Figure 2.11 Schematic diagram of UV-visible spectrophotometer

In the present study UV-visible absorption spectra of the synthesized materials was aquired on "Evaluation 201 Thermo Scientific" using 1 cm path length quartz cuvettes in the wavelength range of 200–700 nm. The photograph of UV-visible spectrophotometer are depicted in (**Figure 2.12**).

Figure 2.12 Typical photograph of UV-visible spectrophotometer

2.7.7. Fluorescence Spectroscopy

Fluorescence is a type of luminescence caused by photons exciting a molecule, raising it to an electronic excited state. It's brought about by absorption of photons in the singlet ground state promoted to a singlet-excited state. As the excited molecule returns to ground state, emits a photon of lower energy, which corresponds to a longer wavelength, than the absorbed photon.

Fluorescence spectroscopy is one of the most versatile, nondestructive highly sensitive spectroscopy technique for probing the electronic structure of materials. Fluorescence spectrophotometer is used to measure the fluorescence or emission intensity and spectral content of the sample which is a direct measure of various important properties sample such as defect and impurities in the sample as well as magnitude of the intensity allows determining their concentration. Moreover, during recording the fluorescence, the excitation, emission or both wavelength may be scanned and the change of signal with temperature, time, polarization and concentration or other variable can be monitored. Fluorescence spectrum is quite differing from absorption spectrum in the sense that absorption spectrum measures the transition from ground state to the excited state whereas fluorescence spectrum deals with transition from excited state to the ground state. Fluorescence spectrum is a graph of emission intensity versus any given excitation wavelength. The wavelength at which molecule shows maximum absorbance can be used as excitation wavelength, which provide a more intense emission at a longer wavelength with a value usually twice of the excitation wavelength. **Figure 2.13** shows the schematic diagram of the key component of fluorescence spectrometer.

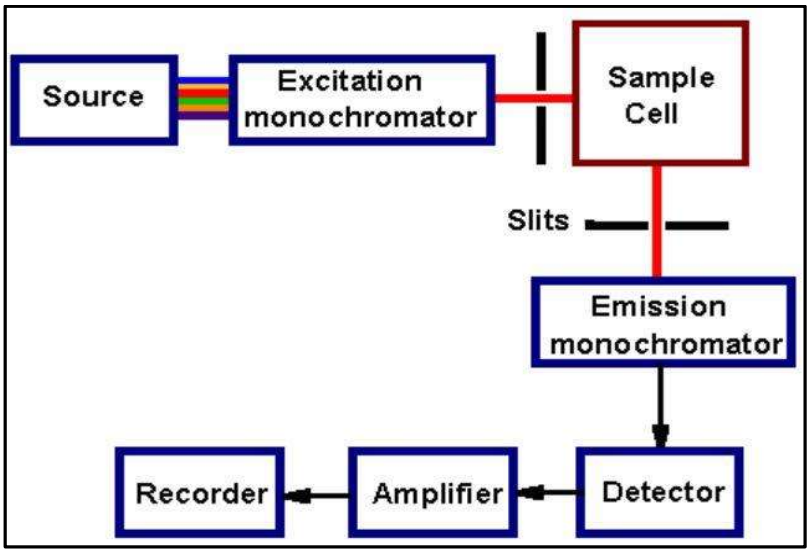

Figure 2.13 Schematic representation of working principle of fluorescence spectrophotometer.

In the present study fluorescence spectrum of materials were recorded on two different Fluorescence Spectrophotometer (Fluoromax 4, Horiba USA), Varian Cary Eclipse Fluorescence Spectrophotometer (**Figure 2.14)**.

Figure 2.14 Photograph of fluorescence spectrophotometer